ADVANCES IN ATMOSPHERIC SCIENCES, VOL. 32, APRIL 2015, 487–496

Future Changes and Uncertainties in Temperature and Precipitation over China Based on CMIP5 Models

TIAN Di, GUO Yan*, and DONG Wenjie

Key Laboratory of Earth Surface Processes and Resource Ecology, Beijing Normal University, Beijing 100875

(Received 15 April 2014; revised 09 July 2014; accepted 28 July 2014)

ABSTRACT

Climate changes in future 21st century China and their uncertainties are evaluated based on 22 climate models from the Coupled Model Intercomparison Project Phase 5 (CMIP5). By 2081–2100, the annual mean surface air temperature (SAT) is predicted to increase by $1.3^{\circ}\mathrm{C} \pm 0.7^{\circ}\mathrm{C}$, $2.6^{\circ}\mathrm{C} \pm 0.8^{\circ}\mathrm{C}$ and $5.2^{\circ}\mathrm{C} \pm 1.2^{\circ}\mathrm{C}$ under the Representative Concentration Pathway (RCP) scenarios RCP2.6, RCP4.5 and RCP8.5, relative to 1986–2005, respectively. The future change in SAT averaged over China increases the most in autumn/winter and the least in spring, while the uncertainty shows little seasonal variation. Spatially, the annual and seasonal mean SAT both show a homogeneous warming pattern across China, with a warming rate increasing from southeastern China to the Tibetan Plateau and northern China, invariant with time and emissions scenario. The associated uncertainty in SAT decreases from northern to southern China. Meanwhile, by 2081–2100, the annual mean precipitation increases by $5\% \pm 5\%$, $8\% \pm 6\%$ and $12\% \pm 8\%$ under RCP2.6, RCP4.5 and RCP8.5, respectively. The national average precipitation anomaly percentage, largest in spring and smallest in winter, and its uncertainty, largest in winter and smallest in autumn, show visible seasonal variations. Although at a low confidence level, a homogeneous wetting pattern is projected across China on the annual mean scale, with a larger increasing percentage in northern China and a weak drying in southern China in the early 21st century. The associated uncertainty is also generally larger in northern China and smaller in southwestern China. In addition, both SAT and precipitation usually show larger seasonal variability on the sub-regional scale compared with the national average.

Key words: CMIP5, China, surface air temperature, precipitation, projection, uncertainty

Citation: Tian, D., Y. Guo, and W. J. Dong, 2015: Future changes and uncertainties in temperature and precipitation over China based on CMIP5 models. *Adv. Atmos. Sci.*, **32**(4), 487–496, doi: 10.1007/s00376-014-4102-7.

1. Introduction

Climate modeling is an important tool for understanding past, present and future climate change (IPCC, 2007; Wang et al., 2008). With large developments in model design since the Coupled Model Intercomparison Project Phase 3 (CMIP3), Phase 5 (CMIP5) provides a new platform for studying the physical mechanisms of climate change, climate projection and predictability. It also provides an important theoretical basis and scientific support for the Intergovernmental Panel on Climate Change's Fifth Assessment Report (IPCC AR5) (Taylor et al., 2012; Wang et al., 2013a). Regional climate change, directly affecting natural and social environments, shows obvious regional differences in the context of global warming, emphasizing the need to study future regional climate changes and their uncertainties based on up-to-date climate models.

Accurate representation of the East Asian monsoon climate is one of the primary difficulties of climate simulations (Sperber et al., 2012; Wei et al., 2013). As a result, China, which is located in the East Asian monsoon region and is also affected by the topography of the Tibetan Plateau, has obvious regional climate variability characteristics. Over the past few decades, changes of the atmospheric circulation due to global warming have been found to affect precipitation and seasonal cycles in China (Lin et al., 2010; Zhu et al., 2010; Yan et al., 2011). Based on CMIP5 models, Chinese researchers have worked hard to assess their general performance, in order to project regional climate over East Asia and China (Xu and Xu, 2012a, b; Zhang, 2012; Chen, 2013; Deng et al., 2013; Guo et al., 2013; Jiang and Tian, 2013; Jiang and Wu, 2013). These studies have demonstrated good performance in representing the main characteristics of the spatial distributions of regional climate, but few have paid significant attention to the uncertainties in the simulations. Chen et al. (2012) predicted increased flooding in China at the end of the 21st century, based on the IPCC's Fourth Assessment Report (AR4) Coupled General Circulation Models (CGCMs). Wang and Chen (2013) analyzed future changes in surface air temperature, precipitation and drought in China under the Representative Concentration Pathway (RCP) scenarios

* Corresponding author: GUO Yan
Email: guoyan@bnu.edu.cn

RCP4.5 and RCP8.5 based on 35 CMIP5 models. Hua et al. (2013) evaluated 24 CMIP3 and 10 CMIP5 simulations of January and July surface air temperature over China and indicated limited capability, especially in July, and larger uncertainty in simulating the climatology, seasonal variability, and trends. Huang et al. (2013) analyzed 14 CMIP5 model simulations of historical summer rainfall in East China and their uncertainties, which showed large model spread in precipitation climatology and seasonal variability. Previous studies have focused on assessing individual climate variables, such as surface air temperature or precipitation, but few have focused on the seasonal variability of climate change, simulated uncertainties, and their regional differences. In this study, we analyze annual and seasonal average climate changes in surface air temperature and precipitation, and their uncertainties, over China and seven climate sub-regions in the 21st century, based on 22 CMIP5 coupled models from 16 international modeling groups. This is intended to deepen understanding of regional climate change in China and the uncertainties in projections.

2. Models and methods

In this study, future climate changes in the early (2016–35), mid (2046–65) and end (2081–2100) of the 21st century are analyzed relative to the present climatology (1986–2005). Outputs of the historical simulation and future projections under RCP2.6, RCP4.5 and RCP8.5 from 22 CMIP5 models (Taylor et al., 2012) are used, and brief model information is listed in Table 1. The historical run simulates the period from 1850 to 2005, forced with time-varying observed anthropogenic and natural forcing agents, including greenhouse gases (CO_2, CH_4, NO_x, O_3, and HF), aerosols (sulfate, nitrate, organic carbon, black carbon, dust, and sea salt), land use, volcanoes, and solar radiation. The future projection runs simulate the period from 2006 to 2100, under RCP2.6, RCP4.5 and RCP8.5, which refer to radiative forcing in 2100 of 2.6, 4.5 and 8.5 W m^{-2}, and CO_2 equivalent mixing ratios of 490, 650 and 1370 ppmv, respectively (Moss et al., 2010; Wang et al., 2012). Here, winter, spring, summer and autumn are December–January–February (DJF), March–April–May (MAM), June–July–August (JJA) and September–October–November (SON) averages, respectively.

The bilinear interpolation method is used to interpolate model outputs with different horizontal resolutions to a $1^\circ \times 1^\circ$ grid. The multi-model ensemble (MME) mean is calculated with equal weight. One inter-model standard deviation (STD) and the inter-model range between the minimum and maximum value are used as metrics to quantify the uncertainty in model projection. In addition, the ratio (signal to noise ratio, Sgl) of the absolute MME (signal) to the inter-model STD (noise) is used to evaluate the credibility of the projected climate change, and the formula is

$$\mathrm{Sgl} = \frac{|\overline{x}|}{\mathrm{STD}} = \frac{|\overline{x}|}{\sqrt{\frac{1}{(n-1)}\sum_{i}^{n}(x_i - \overline{x})^2}},$$

where x_i denotes the ith individual model simulation, $\overline{x}$ denotes the MME, and n is the number of models used. The projection is credible if Sgl is larger than 1 (Zhou and Yu, 2006; Li and Zhou, 2010).

To provide quantitative projection of future climate changes and uncertainties on a sub-regional scale in China, the mainland is divided into seven sub-regions following the work of Wang and Chen (2013) and Huang et al. (2013). These are depicted in Fig. 3, and are: the Tibetan Plateau (TP: altitude greater than 3000 m), Northwest China (NWC: west of 110°E and north of 35°N), Southwest China (SWC: west of 110°E and south of 35°N), Northeast China (NEC: east of 110°E and north of 42°N), North China (NC: 35°–42°N, east of 110°E), East China (EC: 27°–35°N, east of 110°E), and South China (SC: south of 27°N, east of 110°E).

3. Results

3.1. *Surface air temperature*

3.1.1. *Annual mean*

Figure 1a shows the evolution from 1901 to 2100 of the annual mean surface air temperature (SAT) anomalies averaged over China based on the MME with one inter-model STD. It shows that the SAT continues to increase from the 1970s to the end of 21st century under the RCP2.6, RCP4.5 and RCP8.5 scenarios, with the strongest and most contin-

Table 1. Details of the 22 CMIP5 models.

Model	County of origin	Horizontal resolution (lat × lon)	Model	County of origin	Horizontal resolution (lat × lon)
BCC-CSM1-1	China	2.8° × 2.8°	GISS-E2-H	USA	2.5° × 2.0°
BNU-ESM	China	2.8° × 2.8°	GISS-E2-R	USA	2.5° × 2.0°
CanESM2	Canada	2.8° × 2.8°	HadGEM2-AO	South Korea	1.875° × 1.25°
CCSM4	USA	1.25° × 0.94°	IPSL-CM5A-LR	France	3.75° × 1.875°
CNRM-CM5	France	1.4° × 1.4°	IPSL-CM5A-MR	France	2.5° × 1.25°
CSIRO-Mk3-6-0	Australia	1.875° × 1.875°	MIROC5	Japan	1.4° × 1.4°
FGOALS-g2	China	2.8° × 2.8°	MIROC-ESM	Japan	2.8° × 2.8°
FIO-ESM	China	2.8° × 2.8°	MIROC-ESM-CHEM	Japan	2.8° × 2.8°
GFDL-CM3	USA	2.5° × 2.0°	MPI-ESM-LR	Germany	1.9° × 1.9°
GFDL-ESM2G	USA	2.5° × 2.0°	MRI-CGCM3	Japan	1.1° × 1.1°
GFDL-ESM2M	USA	2.5° × 2.0°	NorESM1-M	Norway	2.5° × 1.875°

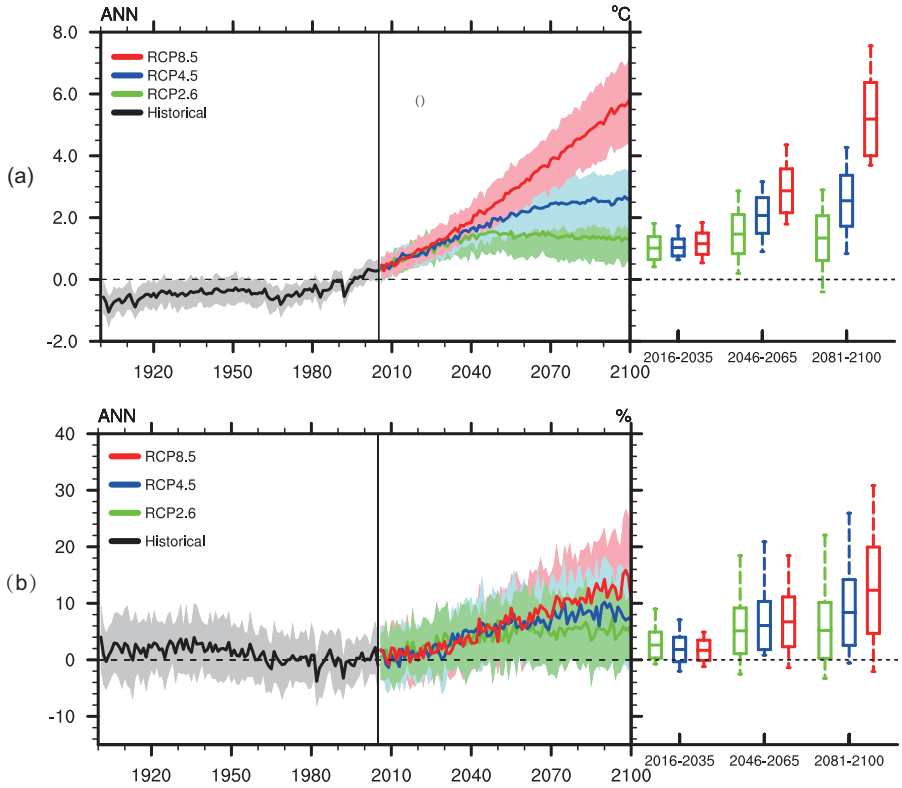

Fig. 1. (a) Annual mean surface air temperature anomalies (units: °C) and (b) precipitation anomaly percentage, averaged over China, relative to 1986–2005, in historical simulations (grey), RCP2.6 (blue), RCP4.5 (green) and RCP8.5 (red) scenarios from the multi-model ensemble (MME) mean (solid line) with one inter-model standard deviation (shading). In the box and whisker plots, the band in the box represents the MME mean, the bottom (top) of the box represents the MME minus (plus) one inter-model standard deviation, and the ends of the whiskers represent the minimum and maximum simulation values.

uous warming under RCP8.5, and flattened or even weakened warming under RCP4.5 and RCP2.6 through the mid 21st century. The SAT difference among the three scenarios is weak in the early 21st century, and gradually increases with integration time. To analyze the uncertainties in SAT projection, the box and whisker plot in Fig. 1a shows one inter-model STD with the MME SAT and inter-model range. The results show a remarkable increase in uncertainty with time under the three emissions scenarios, with the largest uncertainty under RCP8.5 and the smallest under RCP2.6. By the end of the 21st century, the annual mean SAT increases by 1.3°C ± 0.7°C, 2.6°C ± 0.8°C and 5.2°C ± 1.2°C, relative to the present state (1986–2005), under the RCP2.6, RCP4.5, and RCP8.5 scenarios, respectively; the inter-model ranges are −0.4°C to 2.9°C, 0.8°C to 4.3°C, and 3.7°C to 7.6°C, respectively.

Figure 2 shows the spatial distribution of the annual mean SAT changes over China in the early, mid and end of the 21st century, relative to 1986–2005, under the RCP2.6, RCP4.5 and RCP8.5 scenarios. It shows a homogenous warming pattern across China, with greater warming in western and northeastern China, and weaker warming in southeastern China. This pattern resembles the observed pattern of SAT change during the late 20th century found by Ren et al. (2005), Zhou and Yu (2006) and Li et al. (2010). By the end of the 21st century, the increase in the annual mean SAT exceeds 4°C over most of China, and more than 6°C over North Xinjiang, the Tibetan Plateau and northeastern China. There is a certain confidence in the projected SAT changes, as indicated by a signal to noise ratio greater than 1 across all grids over China. In addition, the uncertainty in the SAT projection measured by one inter-model STD is also larger in western and northeastern China than southeastern China (figures not shown for brevity).

The future changes and uncertainties in the annual mean SAT averaged over individual sub-regions in China are shown in Fig. 3. Spatially, the greatest warming is over the TP, followed by NWC, NEC, NC, EC and SC. This forms a spatial structure over China that is generally stable, invariant with emissions scenario and integration time. Taking RCP8.5 as an example, by the end of the 21st century, the annual mean SAT averaged over TP, NWC, NEC, NC, EC, SWC and SC increases by 5.5°C, 5.5°C, 5.5°C, 5.0°C, 4.7°C, 4.5°C and 4.1°C, respectively, with a maximum inter-sub-region discrepancy of 1.4°C.

The uncertainties, in all individual sub-regions, increase with integration time and emissions scenario. Taking NEC as an example, under the RCP8.5 scenario, the uncertain-

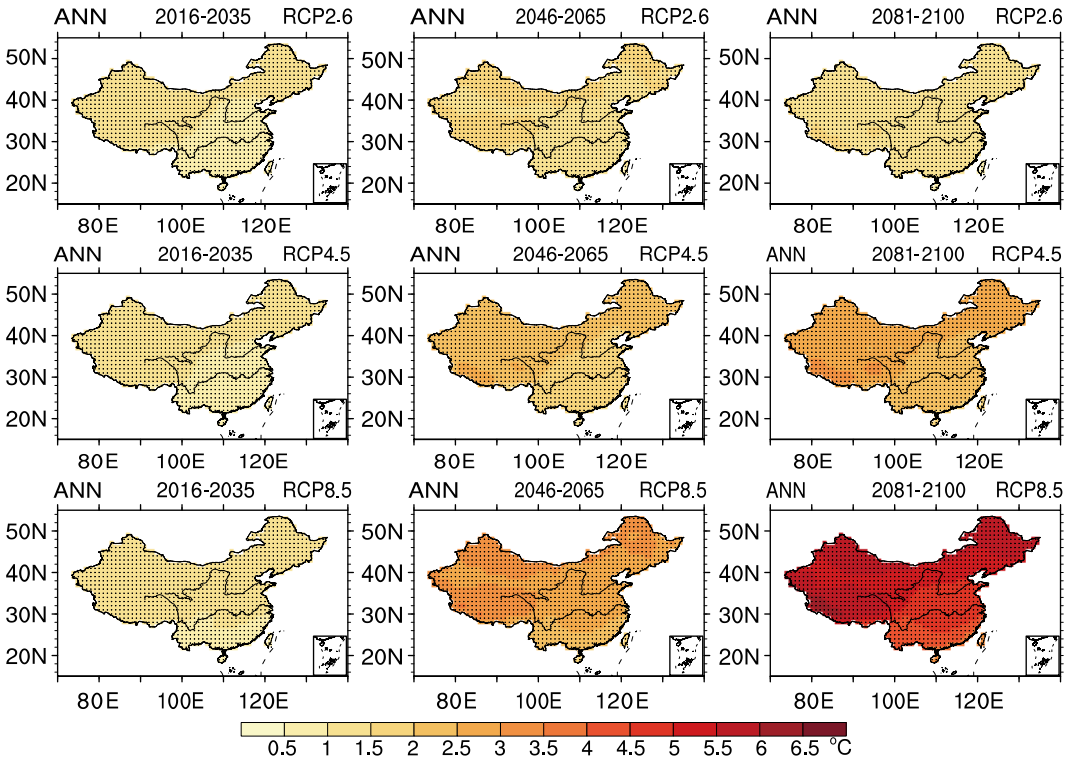

Fig. 2. Spatial distribution of the changes in the annual mean surface air temperature over China in the (left to right) early (2016–35), mid (2046–65) and end (2081–2100) of the 21st century, relative to 1986–2005, under the (top to bottom) RCP2.6, RCP4.5 and RCP8.5 scenarios (units: °C). The black dots denote a signal to noise ratio greater than 1.

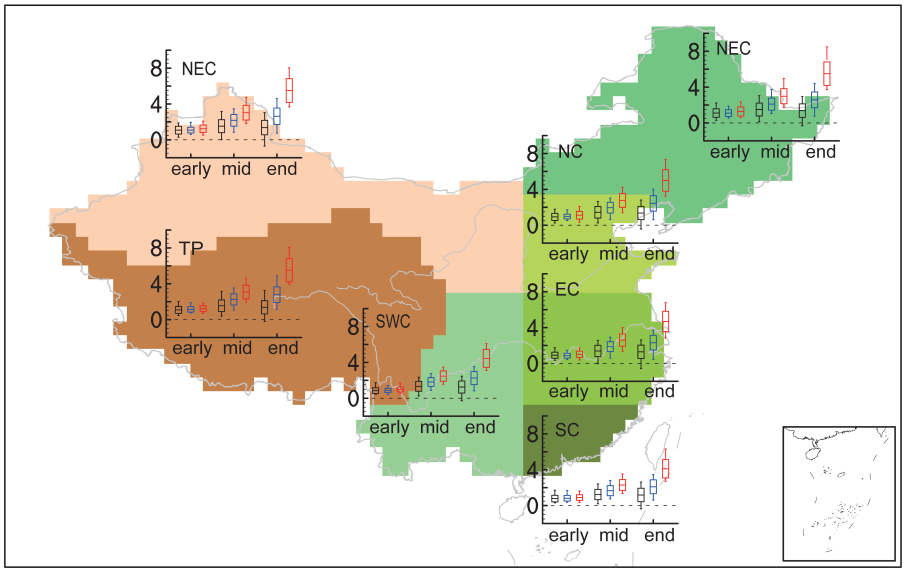

Fig. 3. Changes in the annual mean surface air temperature averaged over the seven sub-regions in China in the early (2016–35), mid (2046–65) and end (2081–2100) of the 21st century, relative to 1986–2005, under the RCP2.6 (black), RCP4.5 (blue) and RCP8.5 (red) scenarios (units: °C). In the box and whisker plots, the band in the box represents the multi-model ensemble (MME) mean, the bottom (top) of the box represents the MME minus (plus) one inter-model standard deviation, and the ends of the whiskers represent the minimum and maximum simulation values. The colored shading represents the distribution of the seven climate divisions over China (TP, Tibetan Plateau; NWC, Northwest China; SWC, Southwest China; NEC, Northeast China; NC, North China; EC, East China; SC, South China).

ties measured by one inter-model STD in the early, mid and end of the 21st century are ±0.5°C, ±0.8°C, and ±1.3°C, respectively; at the end of the century, the uncertainties under RCP2.6, RCP4.5 and RCP8.5 are ±0.8°C, ±0.9°C, and ±1.3°C, respectively. In comparison with the uncertainty in the national average SAT, the uncertainties at a sub-regional scale are larger in the sub-regions over northern China (NEC, NWC, TP, NC) and smaller in the sub-regions over southern China (EC, SC, SWC). Spatially, the largest uncertainty is found in NWC and NEC, followed by TP, NC and EC, and the least in SC and SWC. Taking RCP8.5 as an example, by the end of the 21st century the uncertainties in NWC, NEC, TP, NC, EC, SC and SWC are ±1.3°C, ±1.3°C, ±1.3°C, ±1.2°C, ±1.1°C, ±1.0°C, and ±1.0°C, respectively. In addition, the inter-sub-region discrepancy of uncertainty increases with intensified emissions.

3.1.2. *Seasonality*

The future changes and uncertainties in the SAT averaged over China and individual sub-regions are analyzed from the perspective of seasonality. Figure 4 shows the changes in seasonal mean SAT in the mid 21st century. Future changes in SAT averaged over the whole of China show slight seasonal variations, with the greatest increases of 1.5°C, 2.2°C and 3.0°C in autumn, and the smallest increases of 1.4°C, 2.0°C and 2.7°C in spring under RCP2.6, RCP4.5 and RCP8.5, respectively. In comparison, the sub-regional average SAT shows visible seasonal variation, especially in NEC, followed by NWC, NC, EC and TP, with the least in SWC and SC. In most sub-regions, the seasonality of future SAT is generally consistent under the three emissions scenarios, with the SAT increase greatest in autumn and least in spring. The intensity of the seasonal variation is larger under the RCP8.5 than RCP2.6/RCP4.5 scenario. Spatially, for the seasonal mean SAT, the greatest increase is in northern China (TP, NEC and NWC) and the least in southern China (SWC and SC), forming a spatial pattern across China that is season independent, like the pattern of annual mean SAT. Taking the RCP8.5 scenario as an example, by the middle of the 21st century, the increases in SAT averaged over NEC, TP, NWC, NC, EC, SWC and SC are 3.3°C, 3.1°C, 3.1°C, 2.9°C, 2.9°C, 2.6°C and 2.4°C, respectively in autumn, and 2.5°C, 3.0°C, 2.8°C, 2.5°C, 2.4°C, 2.4°C and 2.3°C, respectively in spring.

The uncertainties in SAT projection averaged over the whole of China show little seasonal variation under the three emissions scenarios. However, on a sub-regional scale, the uncertainty shows certain seasonal variations, whose intensity increases are related to the emissions scenario, and has larger seasonal variability in western than eastern China. Specifically, there is no consistent seasonality in the uncertainties in any individual sub-region or emissions scenario, indicating that seasonal variation of uncertainty is region and emissions-scenario dependent. Spatially, the largest uncertainty is found in northern China (TP, NEC and NWC) and the least in southern China (SWC and SC), forming a spatial pattern that is season independent, like the pattern of uncertainty in annual mean SAT.

The future changes and uncertainties in seasonal mean SAT averaged over China and individual sub-regions at the end of the century are shown in Fig. 5. For the national

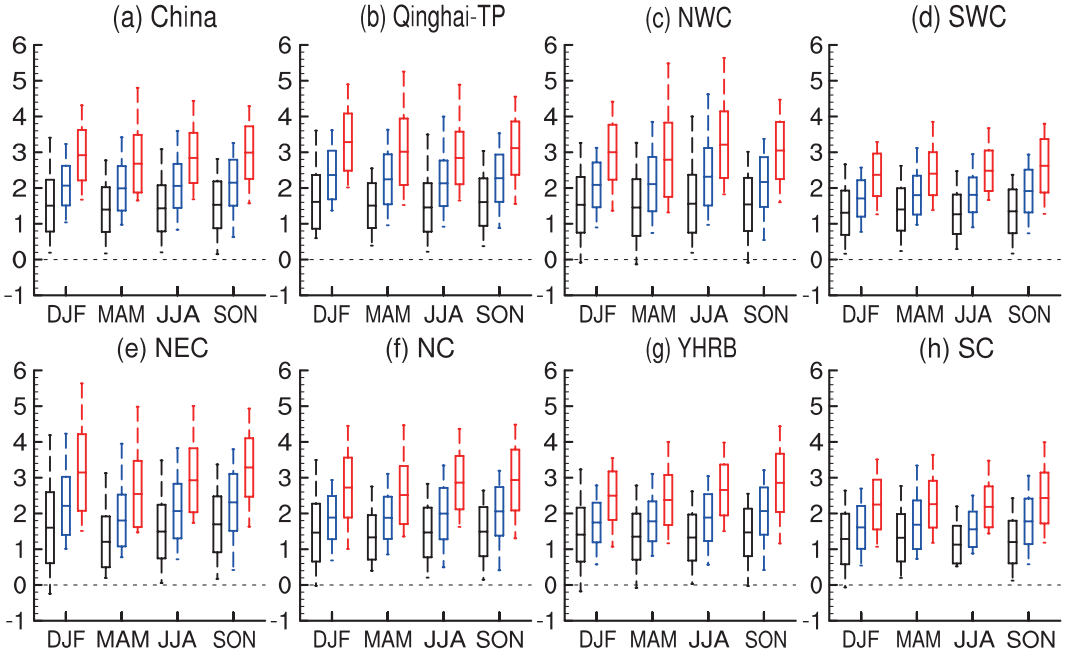

Fig. 4. Changes in the seasonal mean surface air temperature averaged over China and the seven sub-regions in the mid 21st century (2046–65), relative to 1986–2005, under the RCP2.6 (black), RCP4.5 (blue) and RCP8.5 (red) scenarios (units: °C). In the box and whisker plots, the band in the box represents the multi-model ensemble (MME) mean, the bottom (top) of the box represents the MME minus (plus) one inter-model standard deviation, and the ends of the whiskers represent the minimum and maximum simulation values.

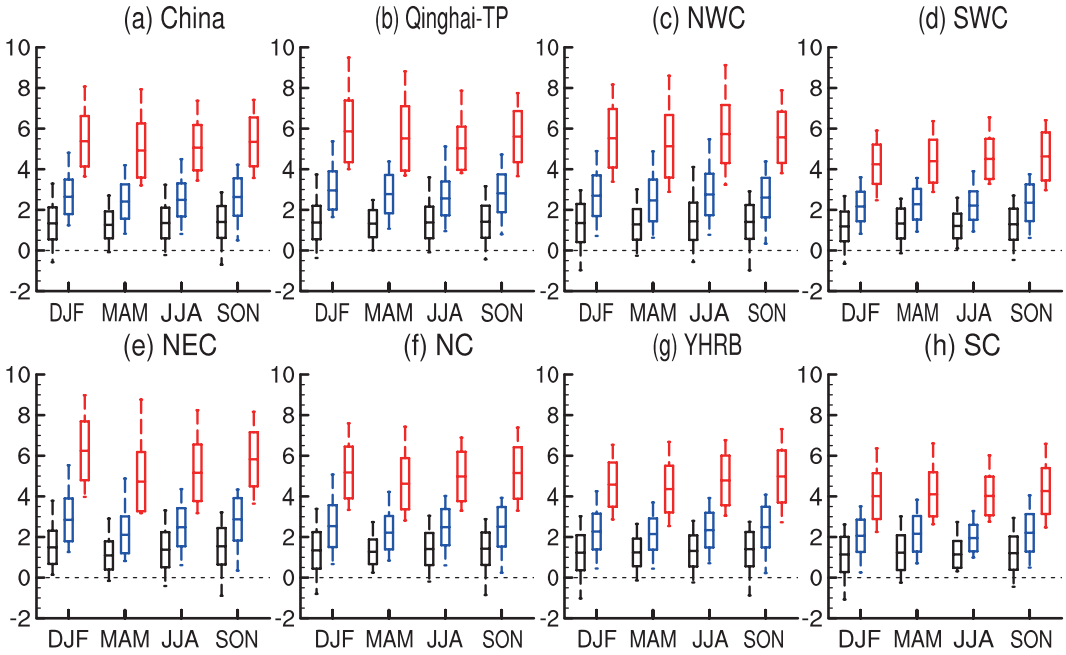

Fig. 5. As in Fig. 4, except for the end of the 21st century (2081–2100) (units: °C).

average SAT, the greatest increase occurs in winter under RCP8.5/RCP4.5 and in autumn under RCP2.6 (5.3°C, 2.6°C and 1.4°C, respectively), and the smallest occurs in spring under RCP8.5, RCP4.5 and RCP2.6 (4.9°C, 2.4°C and 1.3°C, respectively). Under the RCP8.5 scenario, the SAT increases averaged over NEC, TP, NWC, NC, EC, SWC and SC are 6.2°C, 5.9°C, 5.5°C, 5.2°C, 4.6°C, 4.2°C and 4.0°C in winter, and 4.7°C, 5.5°C, 5.1°C, 4.6°C, 4.4°C, 4.4°C and 4.1°C in spring, respectively. The uncertainties in the seasonal mean SAT projection at the end of the century, on national and sub-regional scales, show certain seasonal variations that are region and emissions-scenario dependent.

3.2. *Precipitation anomaly percentage*

3.2.1. *Annual mean*

Figure 1b shows the evolution from 1901 to 2100 of the annual mean precipitation anomaly percentage averaged over China based on the CMIP5 MME with one inter-model STD. It shows that precipitation increases under a background of global warming in the 21st century, with the greatest increases under RCP8.5, and the increases under the RCP2.6 and RCP4.5 scenarios being somewhat flattened. The uncertainty in precipitation projection increases with integration time and emissions scenario. By the end of the 21st century, the annual mean precipitation increases by $5\% \pm 5\%$, $8\% \pm 6\%$ and $12\% \pm 8\%$, relative to the present state (1986–2005), under the RCP2.6, RCP4.5 and RCP8.5 scenarios, respectively; the inter-model ranges are -3% to 22%, -1% to 26% and -2% to 31%, respectively. Note that the change signals of precipitation show less scenario dependence in the early stage of the 21st century. In comparison with the SAT, the increasing rate in precipitation during the 21st century is smaller, but with a larger uncertainty in projection.

Figure 6 shows the spatial distribution of annual mean precipitation anomaly percentage over China in the early, mid and end of the 21st century, relative to 1986–2005, under the RCP2.6, RCP4.5 and RCP8.5 scenarios. The increase in precipitation is widespread across China with a larger percentage in northern China than southern China, except for a weak drying projected in the early 21st century in southern China. Taking the RCP8.5 as an example, at the end of the century the precipitation increase exceeds 15% north of the Yellow River Basin, and as much as 40% in most of northwestern China, whereas the increase is only about 5% in southern China. However, precipitation projection is at a low confidence level, especially for the near-future projection, and spatially for the projection over southern China.

The future changes and uncertainties in the annual mean precipitation anomaly percentage averaged over individual sub-regions in China are shown in Fig. 7. Spatially, the greatest increasing percentage is in NEC, followed by NC, TP and NWC, and the smallest is in SWC and SC, forming a stable spatial structure across China, invariant with emissions scenario and integration time. Taking RCP8.5 as an example, by the end of the century, the annual mean precipitation over NEC, NC, TP, NWC, EC, SWC and SC increase by 19%, 18%, 17%, 15%, 6%, 5% and 3%, respectively, with the maximum inter-sub-region discrepancy reaching 16.5%.

The uncertainties in precipitation projection, over all individual sub-regions, increase with integration time and emissions scenario. Taking NEC as an example, under the RCP8.5 scenario, the uncertainties measured by one inter-model STD in the early, mid and end of the 21st century are $\pm 4\%$, $\pm 7\%$, and $\pm 10\%$, respectively; while at the end of the century, the uncertainties under RCP2.6, RCP4.5 and RCP8.5 are $\pm 7\%$, $\pm 9\%$, and $\pm 10\%$, respectively. The uncertainties in the sub-regional average precipitation are generally larger in comparison with the uncertainty in the national average. The largest

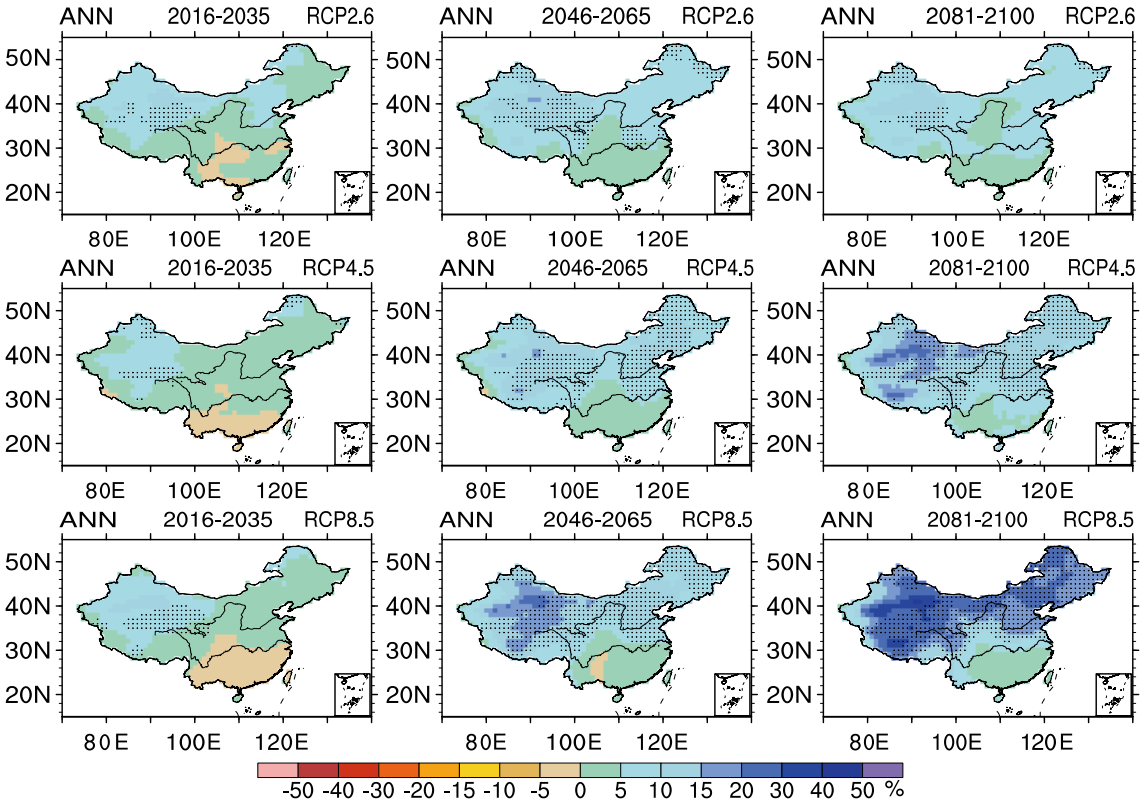

Fig. 6. As in Fig. 2, except for the precipitation anomaly percentage.

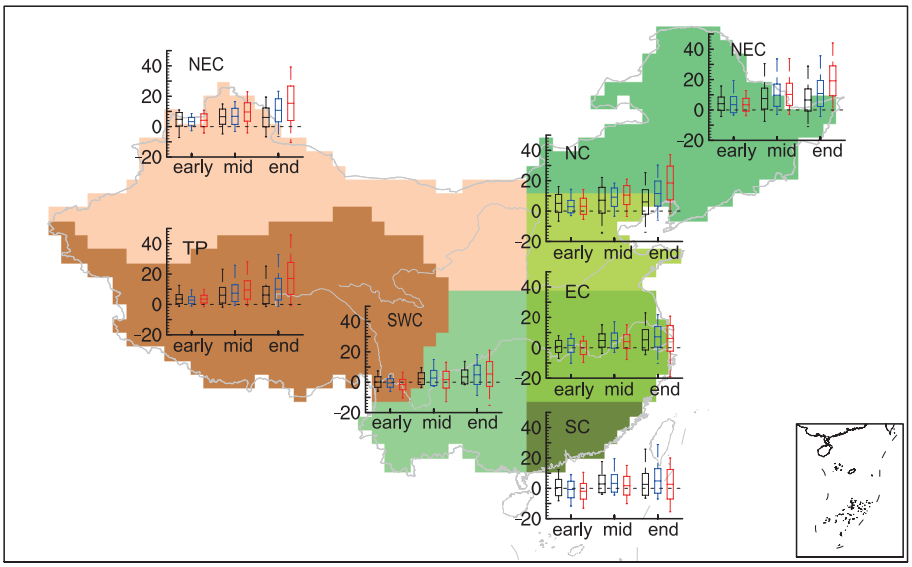

Fig. 7. As in Fig. 3, except for the precipitation anomaly percentage.

uncertainty is found in northern China (NC, NEC), followed by western China (NWC, TP), and southern China (SWC, SC, EC) in the mid and late 21st century; the spatial distribution of uncertainty in precipitation projection is different in the early 21st century.

3.2.2. *Seasonality*

The future changes and uncertainties in the precipitation anomaly percentage averaged over China and the seven sub-regions are analyzed from the perspective of seasonality. Figure 8 shows the changes in the seasonal mean precipitation anomaly percentage in the middle of the 21st century. Future changes in precipitation averaged over the whole of China show evident seasonal variations under the RCP2.6, RCP4.5 and RCP8.5 scenarios, with the largest increasing percentage in spring (7%, 8% and 11%), followed by summer (7%, 8% and 10%), and winter (3%, 5% and 7%). The sub-regional average precipitation also shows a seasonal variation, especially

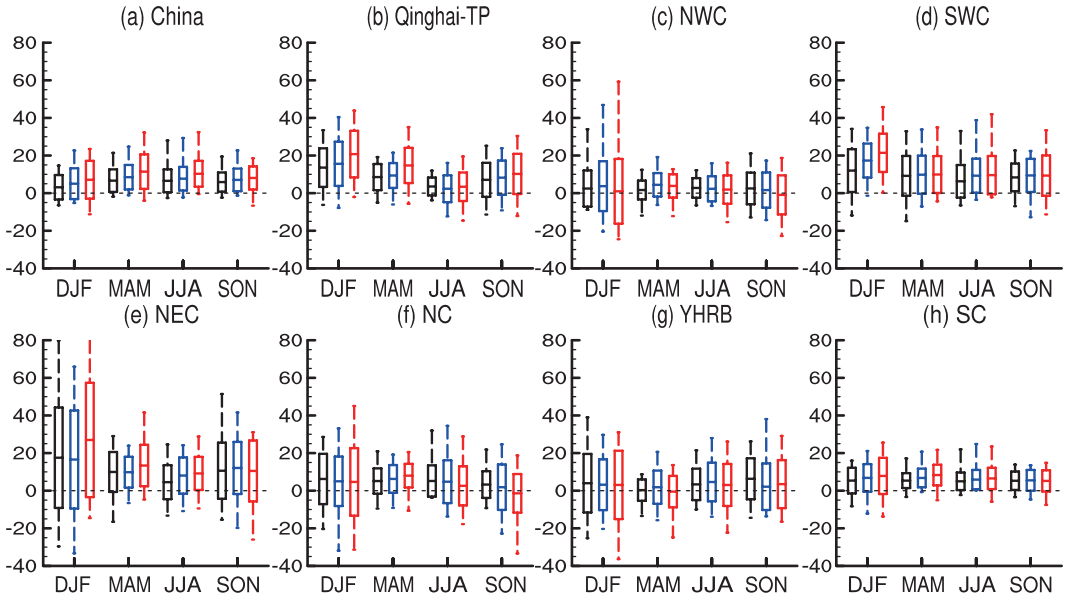

Fig. 8. As in Fig. 4, except for the precipitation anomaly percentage.

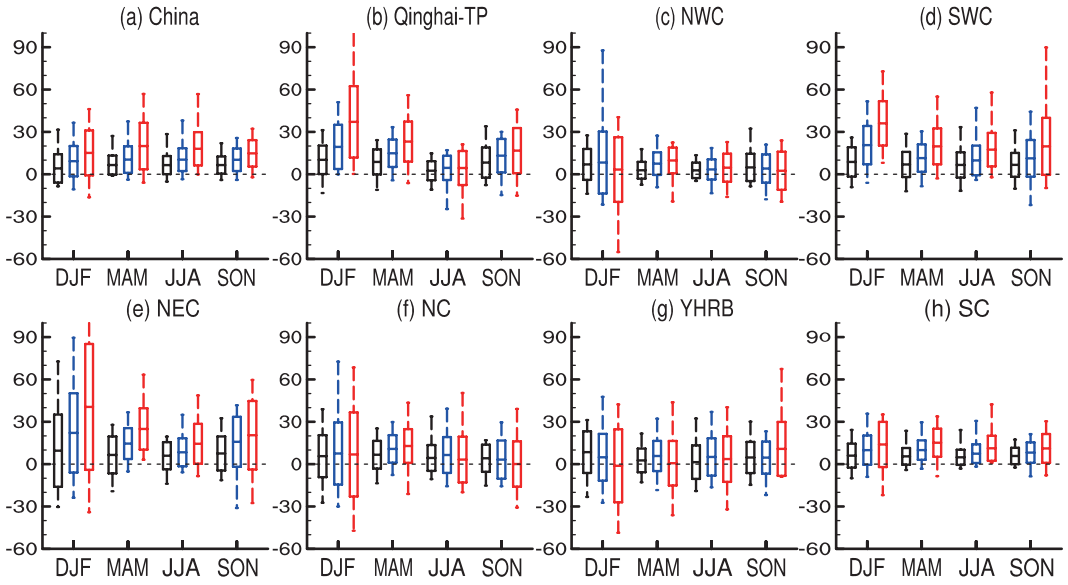

Fig. 9. As in Fig. 5, except for the precipitation anomaly percentage.

in the TP and NEC, followed by SWC, NC and EC, and the least in NWC and SC. However, the seasonality features in the individual sub-regions are different from each other, and vary with emissions scenario. Under the RCP8.5 scenario, by the middle of the century, the precipitation averaged over NEC, SWC, TP, SC, NC, EC, and NWC increases by 27%, 21%, 21%, 8%, 5%, 3% and 1% in winter, and 9%, 10%, 3%, 7%, 3%, 3% and 2% in summer, respectively.

The uncertainty in precipitation projection averaged over the whole of China shows evident seasonal variations under the RCP2.6, RCP4.5 and RCP8.5 scenarios, with the largest uncertainty in winter (±7%, ±8% and ±10%) and the least in autumn (±5%, ±6% and ±6%). The uncertainty in precipitation projection also shows seasonal variation on a sub-regional scale, with larger seasonal variability in northern China than southern China. For individual sub-regions, there is no consistent seasonality in precipitation uncertainty. In most sub-regions, precipitation uncertainty is largest in winter, followed by autumn, and the least in spring.

The future changes and uncertainties in the seasonal mean precipitation anomaly percentage averaged over China and individual sub-regions at the end of the 21st century are shown in Fig. 9. The national average precipitation increases are greatest in spring (7%, 10% and 20% under RCP2.6, RCP4.5 and RCP8.5), followed by summer (6%, 10% and 18%), and smallest in winter (4%, 9% and 15%). The associated uncertainty also shows seasonal variation, with the largest uncertainty in winter (±11% and ±10%)

and the smallest in autumn (±8% and ±6%) under the RCP4.5/RCP2.6 scenario, and with the largest uncertainty in spring (±16%) and the smallest in autumn (±9%) under the RCP8.5 scenario. For individual sub-regions, the seasonal variations of precipitation and associated uncertainties are similar to those in the middle of the century, but with larger amplitudes.

4. Summary and discussion

Based on CMIP5 model outputs from historical simulation and future projections under three RCPs, the future changes and associated uncertainties in SAT and precipitation over China and the seven sub-regions are analyzed on both annual and seasonal mean scales. The main findings are as follows:

The annual mean SAT in China continues to increase from the late 1970s, with strong and continuous warming under RCP8.5, with no or weak warming under the RCP4.5 and RCP2.6 scenarios. The associated uncertainty increases with integration time and emissions scenario. By the end of the 21st century (2081–2100), the annual mean SAT increases by 1.3°C ± 0.7°C, 2.6°C ± 0.8°C and 5.2°C ± 1.2°C, relative to the present state (1986–2005), under the RCP2.6, RCP4.5 and RCP8.5 scenarios, respectively. The annual mean precipitation also increases under a global warming background with a moderate tendency, but a much larger uncertainty in comparison with that of the SAT. By the end of the 21st century, the annual mean precipitation increases by 5% ± 5%, 8% ± 6% and 12% ± 8%, relative to 1986–2005, under the RCP2.6, RCP4.5 and RCP8.5 scenarios, respectively.

The future change in SAT averaged over China increases the most in autumn/winter and the least in spring, while the uncertainty shows little seasonal variation. In comparison, future precipitation changes show visible seasonal variation with the largest increasing percentage in spring, followed by summer, and the least in winter. Seasonal variation is also evident in precipitation uncertainty, with the largest uncertainty in winter and the least in autumn.

Spatially, the annual mean SATs show a homogeneous warming pattern across China with the warming rate increasing from southeastern China to the Tibetan Plateau/northern China, a stable pattern that is invariant with time and emissions scenario. The associated uncertainty in the SAT projection decreases from northern China to southern China. On the seasonal scale, the seasonal mean SAT and its uncertainty basically show the same spatial distribution as the annual mean, but without seasonal dependence. Although the precipitation projection is at a low confidence level, a homogeneous wetting pattern is projected across China on the annual mean scale with a larger increasing percentage in northern China, except for a weak drying in southern China in the early 21st century. The uncertainty in the precipitation projection is generally larger in northern China and smaller in southwestern China, although differences exist in detail as integration time varies.

On the sub-regional scale, the uncertainty in precipitation projection is larger than the national average. In terms of seasonal variations, both the SAT and precipitation show a larger seasonal variability on the sub-regional scale in comparison with the national average. The largest seasonal variability of SAT is found in NEC and NWC, followed by NC, TP, EC, and the smallest in SC and SWC. The largest seasonal variability in the precipitation anomaly percentage is in the TP and NEC, followed by SWC, NC and EC, and the smallest in NWC and SC. As for the seasonal variation of uncertainty, the largest for the SAT projection is in the TP, and for precipitation projection in NEC, NC and NWC.

In this study, the future changes in SAT and precipitation are projected using the most advanced global climate models, which have a coarse resolution and incomplete parameterization in physical process. Thus, a comparison with other projected results obtained from regional climate models (RCMs) or statistical downscaling techniques could provide more confidence in using these results, since the higher resolution afforded by these methods better reproduces the present climate over East Asia (Gao et al., 2001; Ju and Wang, 2006; Yu et al., 2010; Gao et al., 2013). However, they may also introduce further uncertainties (Gao et al., 2012b) that would need addressing in future work. For example, the conclusions regarding the spatial pattern of the SAT responses are similar to those reported by Gao et al. (2012a). Moreover, a detailed comparison of our results with the projected results based on CMIP3 models would also be worthwhile. The uncertainty analyzed in this paper is measured by inter-model discrepancy, and therefore only represents the model uncertainty, i.e., different models produce different responses to the same external forcing, due to differing dynamic frameworks, physical process parameterization schemes, and so on. Other uncertainty sources relevant to the internal variability of the climate system and emissions scenario are not discussed, and may further expand the uncertainty range in the projections. Moreover, Wang et al. (2013b) also pointed out that the summer SAT bias in mid-eastern China is strongly linked to the bias of the Asian Jet Stream based on 22 IPCC AR4 models, implying that further work on model assessment of the major atmospheric circulations in East Asia is necessary.

Acknowledgements. We thank Dr. XU Chonghai for providing the model output data. We thank the anonymous reviewers and editors for their comments. This work is jointly supported by the 973 programs (Grant Nos. 2010CB950501 and 2012CB955501) and the Fundamental Research Funds for the Central Universities (Grant No. 2012LYB43).

REFERENCES

Chen, H. P., 2013: Projected change in extreme rainfall events in China by the end of the 21st century using CMIP5 models. *Chinese Sci. Bull.*, **58**, 1462–1472.

Chen, H. P., J. Q. Sun, X. L. Chen, and W. Zhou, 2012: CGCM projections of heavy rainfall events in China. *Int. J. Climatol.*,

32, 441–450.

Deng, H. Q., Y. Luo, Y. Yao, and C. Liu, 2013: Spring and summer precipitation changes from 1880 to 2011 and the future projections from CMIP5 models in the Yangtze River Basin, China. *Quaternary International*, **304**, 95–106.

Gao, X. J., Z. C. Zhao, Y. H. Ding, R. H. Huang, and F. Giorgi, 2001: Climate change due to greenhouse effects in China as simulated by a regional climate model. *Adv. Atmos. Sci.*, **18**, 1224–1230, doi: 10.1007/s00376-001-0036-y.

Gao, X., Y. Xu, Z. Zhao, J. S. Pal, and F. Giorgi, 2006: On the role of resolution and topography in the simulation of East Asia precipitation. *Theor. Appl. Climatol.*, **86**, 173–185.

Gao, X. J., Y. Shi, D. F. Zhang, and F. Giorgi, 2012a: Climate change in China in the 21st century as simulated by a high resolution regional climate model. *Chinese Sci. Bull.*, **57**, 1188–1195.

Gao, X. J., Y. Shi, D. F. Zhang, J. Wu, F. Giorgi, Z. M. Ji, and Y. G. Wang, 2012b: Uncertainties in monsoon precipitation projections over China: Results from two high-resolution RCM simulations. *Climate Res.*, **52**, 213–226.

Gao, X. J., M. L. Wang, and F. Giorgi, 2013: Climate change over China in the 21st century as simulated by BCC_CSM1.1-RegCM4.0. *Atmos. Oceanic Sci. Lett.*, **6**, 381–386.

Guo, Y., W. J. Dong, F. M. Ren, and J. B. Huang, 2013: Surface air temperature simulations over China with CMIP5 and CMIP3. *Advances in Climate Change Research*, **4**, 145–152.

Hua, W. J., H. J. Chen, and S. L. Sun, 2013: Uncertainty in land surface temperature simulation over China by CMIP3/CMIP5 models. *Theor. Appl. Climatol.*, **117**, 463–474.

Huang, D. Q., J. Zhu, Y. C. Zhang, and A. N. Huang, 2013: Uncertainties on the simulated summer precipitation over Eastern China from the CMIP5 models. *J. Geophys. Res.*, **118**, 9035–9047.

IPCC, 2007: *The Physical Science Basis: Contribution of Working Group I to the Fourth Assessment Report of the Intergovernmental Panel on Climate Change*, Solomon et al., Eds., Cambridge University Press, 996 pp.

Jiang, D. B., and Z. P. Tian, 2013: East Asian monsoon change for the 21st century: Results of CMIP3 and CMIP5 models. *Chinese Sci. Bull.*, **58**, 1427–1435.

Jiang, Y. M., and H. H. Wu, 2013: Simulation capabilities of 20 CMIP5 models for annual mean air temperatures in Central Asia. *Advances in Climate Change Research*, **9**, 110–116. (in Chinese)

Ju, L. X., and H. J. Wang, 2006: Modern climate over East Asia simulated by a regional climate model nested in a global grid-point general circulation model. *Chinese J. Geophys.*, **49**, 52–60. (in Chinese)

Li, B., and T. J. Zhou, 2010: Projected climate change over China under SRES A1B scenario: Multi-model ensemble and uncertainties. *Advances in Climate Change Research*, **6**, 270–276.

Li, Q. X., W. J. Dong, W. Li, X. R. Gao, P. Jones, J. Kennedy, and D. Parker, 2010: Assessment of the uncertainties in temperature change in China during the last century. *Chinese Sci. Bull.*, **55**, 1974–1982. (in Chinese)

Lin, Z. D., R. Y. Lu, and W. Zhou, 2010: Change in early-summer meridional teleconnection over the western North Pacific and East Asia around the late 1970s. *Int. J. Climatol.*, **30**, 2195–2204.

Moss, R. H., and Coauthors, 2010: The next generation of scenarios for climate change research and assessment. *Nature*, **463**, 747–756.

Ren, G. Y., and Coauthors, 2005: Recent progresses in studies of regional temperature changes in China. *Climatic and Environmental Research*, **10**, 701–716. (in Chinese)

Sperber, K. R., H. Annamalai, I.-S. Kang, A. Kitoh, A. Moise, A. Turner, B. Wang, and T. Zhou, 2012: The Asian summer monsoon: An intercomparison of CMIP5 vs. CMIP3 simulations of the late 20th century. *Climate Dyn.*, **41**, 2711–2744.

Taylor, K. E., R. J. Stouffer, and G. A. Meehl, 2012: An overview of CMIP5 and the experiment design. *Bull. Amer. Meteor. Soc.*, **93**, 485–498.

Wang, B., T. J. Zhou, Y. Q. Yu, and B. Wang, 2008: A perspective on earth system model development. *Acta Meteorologica Sinica*, **66**, 857–869. (in Chinese)

Wang, L., and W. Chen, 2013: A CMIP5 multimodel projection of future temperature, precipitation, and climatological drought in China. *Int. J. Climatol.*, **34**, 2059–2078.

Wang, S. W., Y. Luo, Z. C. Zhao, X. Y. Wen, and J. B. Huang, 2012: New generation of scenarios of greenhouse gas emission. *Advances Climate Change Research*, **8**, 305–307. (in Chinese)

Wang, S. W., Y. Luo, Z. C. Zhao, X. Y. Wen, and J. B. Huang, 2013a: Climate model. *Advances in Climate Change Research*, **9**, 150–154. (in Chinese)

Wang, X., W. Zhou, D. X. Wang, and C. Z. Wang, 2013b: The impacts of the summer Asian Jet Stream biases on surface air temperature in mid-eastern China in IPCC AR4 models. *Int. J. Climatol.*, **33**, 265–276.

Wei, K., T. Xu, Z. C. Du, H. N. Gong, and B. H. Xie, 2013: How well do the current state-of-the-art CMIP5 models characterise the climatology of the East Asian winter monsoon? *Climate Dyn.*, doi: 10.1007/s00382-013-1929-z.

Xu, C. H., and Y. Xu, 2012a: The projection of temperature and precipitation over China under RCP scenarios using a CMIP5 multi-model ensemble. *Atmos. Oceanic Sci. Lett.*, **5**, 527–533.

Xu, Y., and C. H. Xu, 2012b: Preliminary assessment of simulations of climate changes over China by CMIP5 Multi-Models. *Atmos. Oceanic Sci. Lett.*, **5**, 489–494.

Yan, Z. W., J. J. Xia, C. Qian, and W. Zhou, 2011: Changes in seasonal cycle and extremes in China during the period 1960–2008. *Adv. Atmos. Sci.*, **28**, 269–283, doi: 10.1007/s00376-010-0006-3.

Yu, E. T., H. J. Wang, and J. Q. Sun, 2010: A quick report on a dynamical downscaling simulation over China using the nested model. *Atmos. Oceanic Sci. Lett.*, **3**, 325–329.

Zhang, Y., 2012: Projections of 2.0°C warming over the globe and China under RCP4.5. *Atmos. Oceanic Sci. Lett.*, **5**, 514–520.

Zhou, T. J., and R. C. Yu, 2006: Twentieth-Century surface air temperature over China and the globe simulated by coupled climate models. *J. Climate*, **19**, 5843–5858.

Zhu, Y. L., H. J. Wang, W. Zhou, and J. H. Ma, 2010: Recent changes in the summer precipitation pattern in East China and the background circulation. *Climate Dyn.*, **36**, 1463–1473.